Available online at www.sciencedirect.com
ScienceDirect
Polar Science 1 (2007) 85–100
http://ees.elsevier.com/polar/

New insight into the crust and upper mantle structure under Alaska

Cheng Qi [a,b,*], Dapeng Zhao [a], Yong Chen [c], Natalia A. Ruppert [d]

[a] *Department of Geophysics, Tohoku University, Sendai 980-8578, Japan*
[b] *Institute of Geology and Geophysics, Chinese Academy of Science, Beijing 100029, China*
[c] *Institute of Earthquake Science, China Earthquake Administration, Beijing, China*
[d] *Geophysical Institute, University of Alaska, Fairbanks, USA*

Received 9 March 2007; revised 29 June 2007; accepted 3 July 2007
Available online 10 October 2007

Abstract

To better understand the seismic structure of the subducting Pacific plate under Alaska, we determined the three-dimensional P-wave velocity structure to a depth of approximately 200 km beneath Alaska using 438,146 P-wave arrival times from 10,900 earthquakes. In this study an irregular grid parameterization was adopted to express the velocity structure under Alaska. The number of grid nodes increases from north to south in the study area so that the spacing between grid nodes is approximately the same in the longitude direction. Our results suggest that the subducting Pacific slab under Alaska can be divided into three different parts based on its geometry and velocity structure. The western part has features similar to those in other subduction zones. In the central part a thick low-velocity zone is imaged at the top of the subducting Pacific slab beneath north of the Kenai Peninsula, which is believed to be most likely the oceanic crust plus an overlying serpentinized zone and the coupled Yakutat terrane subducted with the Pacific slab. In the eastern part, significant high-velocity anomalies are visible to 60–90 km depth, suggesting that the Pacific slab has only subducted down to that depth.

Keywords: Seismic tomography; Subduction zone; Alaska; Yakutat terrane; Arc volcanism

1. Introduction

Alaska is located at the northern end of the active plate boundary between the Pacific plate and the North American plate. The Pacific plate subducts northwestwards beneath south-central Alaska at a rate of about 54 mm/year (Brocher et al., 1994), which leads to the formation of an island arc in the Alaska Peninsula in western Alaska. However, in southern and eastern Alaska the situation is more complex. The direction of subduction changes from normal in the central Aleutians to oblique beneath the transition zone and the Wrangell subduction zone is characterized as right-lateral strike-slip faulting on the surface along the Queen Charlotte/Fairweather fault system east of 136°W (Lahr and Plafker, 1980; Stephens et al., 1984; Page et al., 1989) (Fig. 1).

* Corresponding author. Department of Geophysics, Tohoku University, Sendai 980-8578, Japan.
E-mail addresses: qicheng@mail.iggcas.ac.cn (C. Qi), zhao@aob.geophys.tohoku.ac.jp (D. Zhao).

1873-9652/$ - see front matter © 2007 Elsevier B.V. and NIPR. All rights reserved.
doi:10.1016/j.polar.2007.07.001

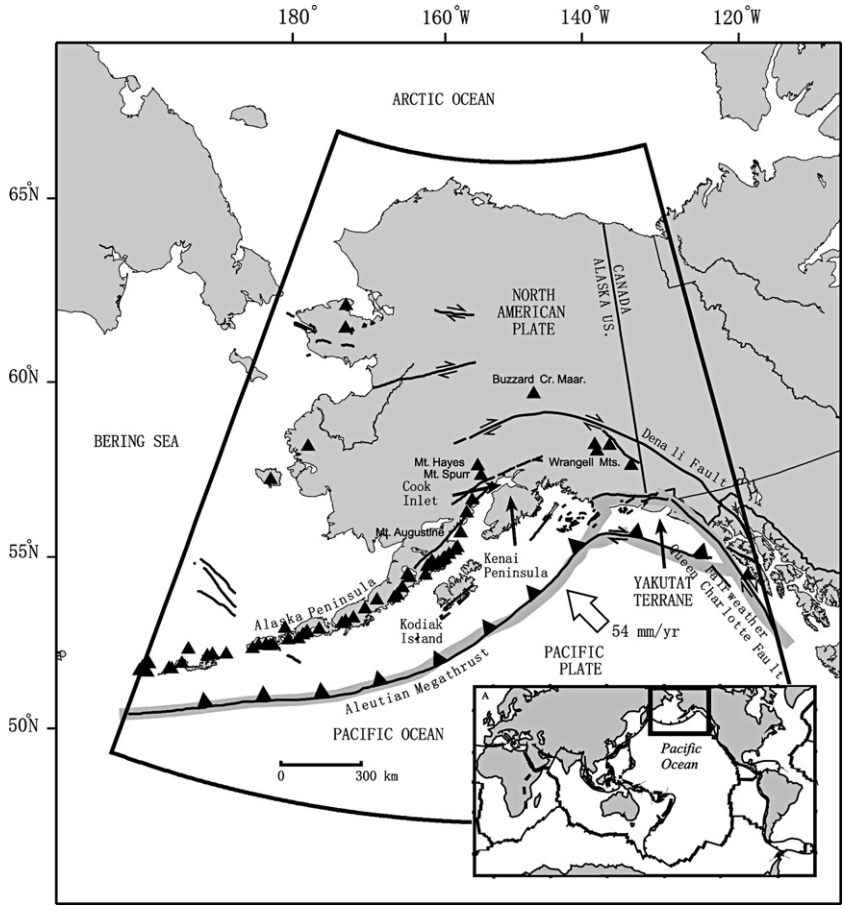

Fig. 1. Map showing the main tectonic framework around Alaska and some location names. The Pacific plate subducts northwestwards beneath south-central Alaska at a rate of about 54 mm/year (Brocher et al., 1994). The faults are shown as the lines with various lengths. The heavy black lines encircle the range of the study area. The inserted map in the lower right corner shows the location of the present study region in the world map with plate boundaries indicated.

As a result of the subduction of an oceanic plate that carried several continental fragments, southern Alaska is composed of a series of terranes with different origins (Jones et al., 1987). Among these terranes, the Yakutat terrane is frequently studied and is regarded as the linchpin to understanding the geodynamic process of the subduction zone in this region (see Fig. 1). Currently in the Gulf of Alaska, the Pacific plate and the overlying Yakutat terrane are subducting beneath and colliding with the North American plate (Plafker, 1987). Furthermore, a series of distinct phenomena in this area, such as the world's shallowest dip angle of subduction, the Yakataga seismic gap (Page et al., 1989) and the Denali volcanic gap (Nye, 1999), make this complicated region more intriguing.

Although the tectonic characteristics of Alaska are complicated, the subducting Pacific slab under Alaska should exhibit strong seismic velocity anomalies and so is very suitable for a tomographic study. Kissling and Lahr (1991) and Zhao et al. (1995) produced the first tomographic images of Alaska, revealing high-velocity (high-V) anomalies corresponding to the subducting Pacific slab and low-velocity (low-V) anomalies in the mantle wedge under the active arc volcanoes. However, in comparison with other well-studied subduction zones such as Japan (e.g., Zhao et al., 1992, 1994), the two Alaskan studies could not image well the slab structure under Alaska. Recently, Eberhart-Phillips et al. (2006) combined local earthquakes and active source data to improve the seismic image of south-central Alaska and obtained better results. In particular, a thick low-V zone at the top of the subducting Pacific slab beneath north of Cook Inlet is further confirmed, and this low-V zone is suggested to be related to the Yakutat terrane subducted along with the Pacific slab.

In this work, we used a large number of arrival times recorded by the Alaska Earthquake Information Center (AEIC) during the last 25 years to determine a detailed P-wave velocity structure under the entire Alaska down to 190 km depth, and revealed new structure features of the Alaska subduction zone. We modified the tomographic inversion program of Zhao et al. (1992) by adopting an irregular grid parameterization to express the 3-D velocity structure under Alaska. Thus the spacing between grid nodes is approximately the same in the longitude direction, allowing the tomographic inversion to have more feasibility for polar regions such as Alaska.

2. Data and method

The abundant seismicity in Alaska and the dense seismic network including permanent and temporary seismic stations as well as a long history of data collection provide an outstanding data set for this tomographic study. We used first P and S arrival times recorded by ~500 AEIC permanent and temporary seismic stations that operated for various scientific research projects from January 1977 to December 2002 in the Alaska region (Figs. 2 and 3). The majority of the stations are located in south-central Alaska (Fig. 3), and the earthquakes are mostly clustered in the upper crust and in the Wadati-Benioff zone (WBZ) to a depth of about 200 km (Fig. 2).

Earthquake selection is based on the following criteria. (1) Events with clear P arrivals recorded at more than seven stations. However in the crucial areas of low seismicity, events with six P and three S arrivals were also selected; (2) events with formal mislocation errors less than 5 km, although most had much smaller errors; (3) to achieve a uniform event distribution, earthquakes were filtered by small boxes with a size of $0.1^\circ \times 0.1^\circ \times 2$ km. In each box only the event with the greatest number of first P arrivals was selected.

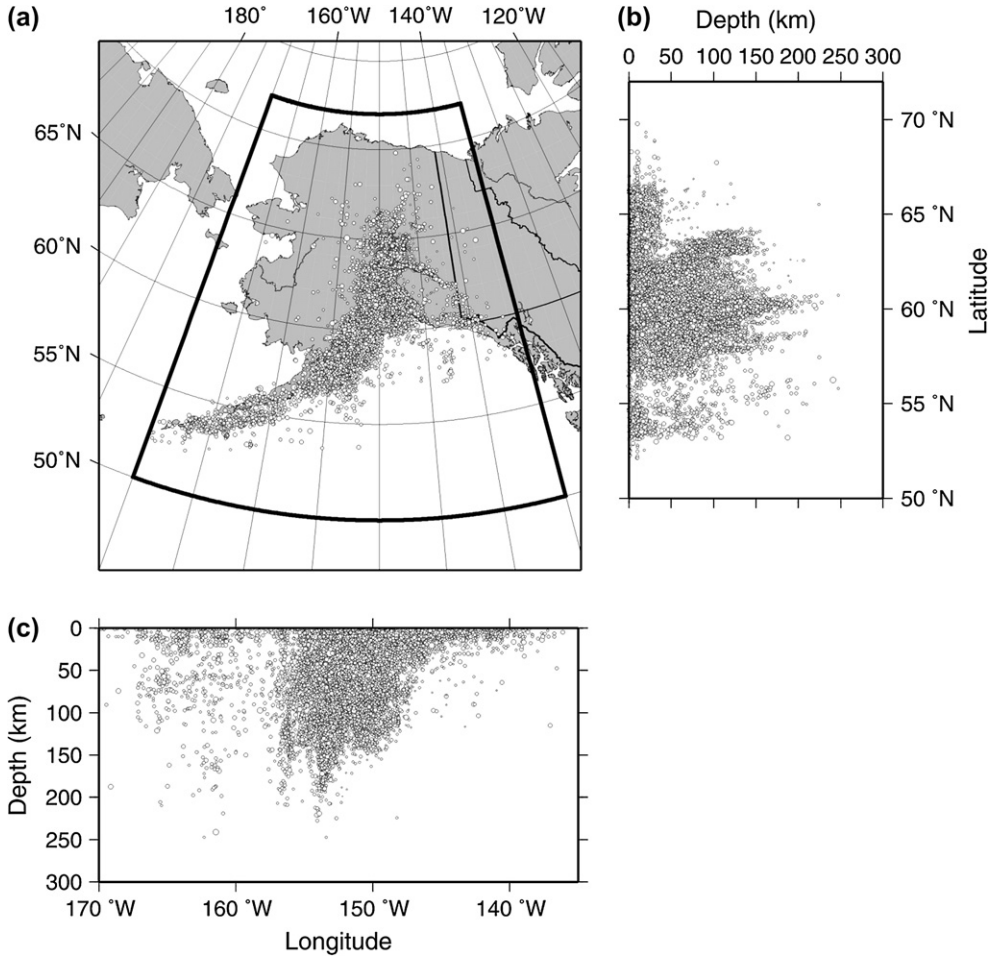

Fig. 2. Hypocentral distribution of earthquakes (circles) used in this study.

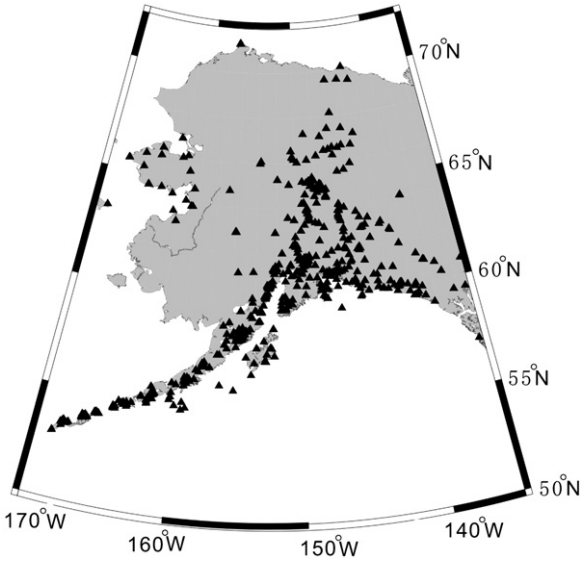

Fig. 3. Map showing the locations of seismic stations (black triangles) used in this study.

As a result, 10,900 earthquakes were selected. The total number of P arrivals was 438,146 and that of S arrivals was 118,858. S arrivals were only used to relocate earthquakes together with P arrivals and were not used for tomographic inversion. Comparing with a previous similar study in this region (Zhao et al., 1995, who used 142,908 P-wave data), this study had more data of higher quality. The accuracy of arrival times was estimated to be 0.1–0.2 s for most of the data. The arrival times were corrected for the ellipticity of the Earth (Dziewonski and Gilbert, 1976).

To analyze the arrival time data, the tomographic method of Zhao et al. (1992) was adopted. This method has been used in many tomographic studies of regions with different tectonic backgrounds, and has particularly given good results for subduction zones (e.g., Zhao et al., 1992, 1997).

Alaska is located in the high latitude region near the North Pole. It is not appropriate to adopt a conventional regular grid parameterization on the basis of the Earth's longitude and latitude coordinate system. For example, in the adopted model with regular grid parameterization, the distance between two grid nodes separated by 1° in longitude at 50°N latitude is ~71.55 km. However, the distance is reduced to only ~38.12 km at 70°N latitude. The grid nodes become closer to one another nearer the North Pole (see Fig. 4).

In the present study, we have modified the computer program of Zhao et al. (1995) according to the special geographic location of Alaska. Instead of the regular grid parameterization, an irregular grid parameterization was adopted to express the velocity structure. In this velocity model the number of grid nodes increases from north to south in the study area so that the spacing between grid nodes is approximately the same in the longitude direction.

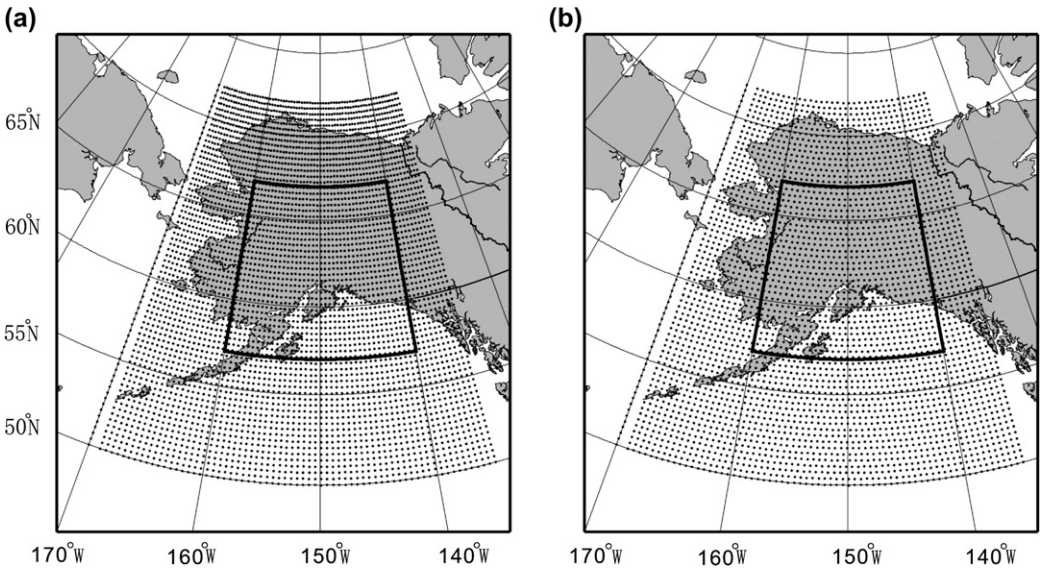

Fig. 4. Configurations of the grid net in the horizontal plane in models with (a) the regular and (b) irregular grid parameterization. The boxes show the range of the region shown in Fig. 6.

3. Analysis

First we show the test results of the modified inversion program. In Fig. 5 we compare the results of seismic ray tracing in the case of direct P and Pn waves in the regular and irregular grid models. For details of the 3-D ray tracing technique, see Zhao et al. (1992). The test results show that the seismic ray paths and travel times are exactly the same in the two models, suggesting that the seismic ray tracing is completely independent of the grid parameterization, which is very important.

According to the distributions of events and stations used in this study, the region in the longitude range of ∼170–135°W, latitude range of ∼50–72°N, and depth range of ∼0–190 km is taken as the model space.

Referring to the initial P-wave 1-D velocity model in the previous study (Zhao et al., 1995), in this study P-wave velocities of the upper crust, lower crust, and uppermost mantle are defined as 6.0, 6.7, and 7.9 km/s, respectively. For the upper mantle, we used the iasp91 Earth model (Kennett and Engdahl, 1991). The depths to the Conrad and Moho discontinuities are 13.0 and 36.5 km, respectively.

Velocity perturbations at grid nodes from the 1-D velocity model are considered as unknown parameters. The velocity perturbation at any point in the model is computed by linearly interpolating the velocity perturbations at the nearest eight grid nodes surrounding that point. The efficient 3-D ray tracing technique (Zhao et al., 1992) and derivative computation associated with the unknown parameters, which is used to construct the observation equations, are included in

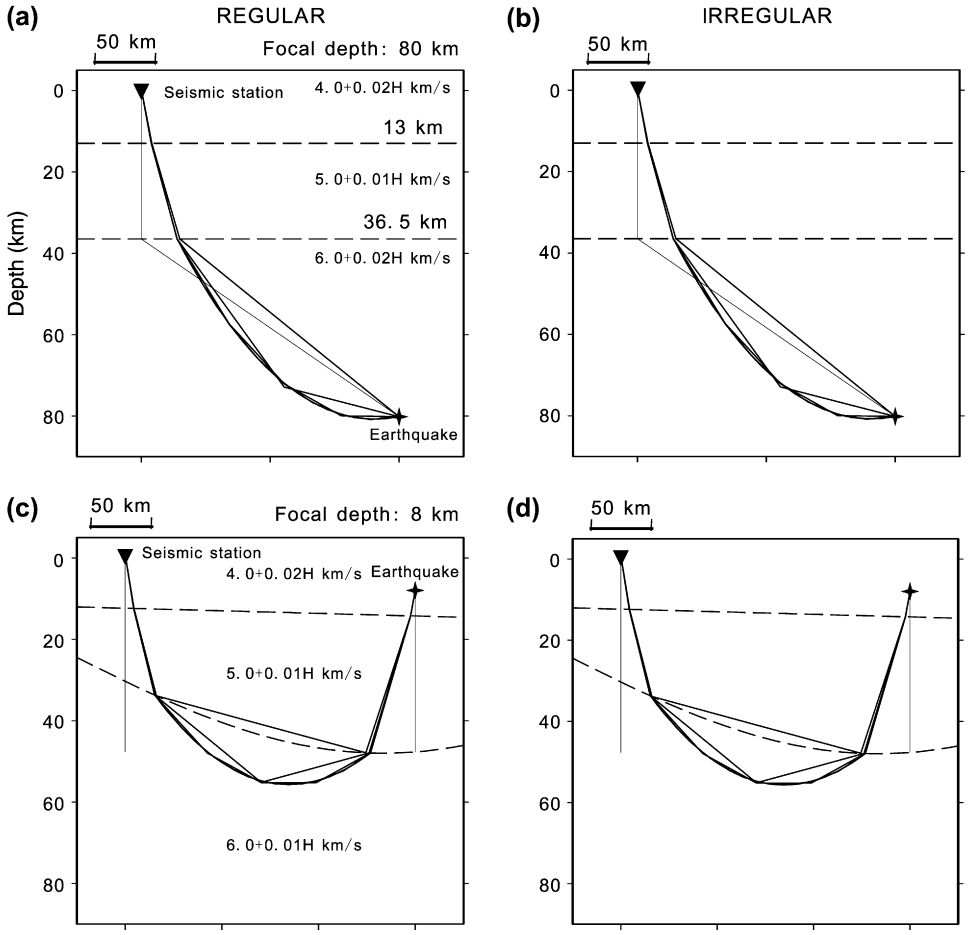

Fig. 5. Comparison of the ray paths in the models with (a and c) the regular and (b and d) irregular grid parameterization. Lines indicate the snapshots of the seismic ray paths in each step of the ray-tracing calculation (see Zhao et al., 1992). Dashed lines are velocity discontinuities. The seismic velocities in each layer are shown in (a).

the inversion. According to the irregular grid parameterization being used, these related problems in the program were also dealt with. The LSQR algorithm (Paige and Saunders, 1982) with damping and smoothing was used to conduct inversions of the observation equations. The nonlinear tomographic problem is solved by iteratively conducting linear inversions.

Many models with different grid spacing were tried. According to the results of the checkerboard resolution tests, a grid spacing of 0.25° (hereinafter the unit of degree is taken as the distance in degrees along the great circle path, not a latitude or longitude measurement) is finally chosen, which is ∼28 km on the Earth's surface. In the depth direction, 9 layers are adopted, the same as those in the previous similar study (Zhao et al., 1995).

In this study, we conducted a number of inversions with different damping and smoothness parameters. According to the trade-off between root-mean-square (RMS) travel time residual and model variance, appropriate damping and smoothness parameters were selected to obtain a reliable and coherent result. The velocity structure and hypocentral locations are simultaneously determined in the inversion process.

The checkerboard resolution test (CRT, Humphreys and Clayton, 1988; Zhao et al., 1992) is normally used to assess the adequacy of the ray coverage and to evaluate the final resolution as well as for making further model adjustments as mentioned above. In Fig. 6, results of two checkerboard resolution tests with regular and irregular grid models are compared at 40 km depth. In the irregular grid model, it is not easy to discern the checkerboard pattern. A better method is to use a relative variation measurement, i.e., the ratio of the inverted model to the input checkerboard model. At the bottom of Fig. 6, star and cross symbols indicate positive and negative values of the ratios, respectively. The larger the star (cross) symbols are, the better (worse) the reconstructed result is. Generally speaking, the resolution of a tomographic image decreases when a smaller grid spacing is adopted. In the regular grid model, it is very easy to understand that the resolution is poor in the north. However, in the irregular grid model, since a larger spacing between grid nodes is used relative to that in the regular grid model, the checkerboard image is better reconstructed; not only the pattern but also the amplitude of velocity anomalies are better recovered.

Fig. 7 shows the results of a CRT. Random errors in a normal distribution with a standard deviation of 0.1 s are added to arrival times calculated for the synthetic models. As mentioned above, stars represent good resolution. Here we show three typical layers of two different results with grid spacings of 0.25° and 0.33°. Most of the layers are of good resolution. The resolution is generally high in the central part of the study area, particularly along the subducting Pacific slab. The resolution of intermediate-depth layers is better than that of other layers. From the two resolution tests with different grid spacings we can say that the tomographic image obtained in the present study has a spatial resolution of 0.25–0.33°. Anomalies of larger size than this can be discerned reliably.

To further confirm the reliability of the final images and the geometry of the subducting Pacific plate in particular, a synthetic resolution test with a specific structural geometry and a restoring resolution test (RRT, Zhao et al., 1992) were also used in this study. In the synthetic resolution test, a slab-like anomaly with a width of 50 km and 2% higher velocity than its surroundings was introduced into the initial 1-D model. We call the modified model the ''input model''. As for the RRT, we take the tomographic image obtained by inverting the real data set as the input model. Synthetic arrival times are then calculated by three-dimensionally tracing rays in the observed data set for the input models. The same random error as that used in the CRT is also added to the calculated synthetic data. By inverting the synthetic data using the same inversion procedure, we obtained the recovered images which are called ''output models''. Comparing the input models with the output models, we can know how well the main trend or some special structures in the real result are realistically reconstructed. Fig. 8 shows two examples with input models and output models obtained by the synthetic test (Fig. 8a and b) and RRT (Fig. 8c and d), respectively.

Zhao et al. (1995) introduced a priori high-V subducting Pacific slab into the model and called the inversions ''slab inversions''. For the sake of convenience in calculations, they simply estimated the depth of the slab surface in the transition zone where no intermediate-depth earthquakes occur between 144.5°W and 149°W, according to the closest known depth contours of the slab surface (Zhao et al., 1995), i.e., the Alaska–Aleutian subduction zone to the west and the Wrangell subduction zone to the east (see Fig. 9). Actually, due to insufficient evidence in the transition zone and the Wrangell region (141°W to 144.5°W), the location of the upper boundary of the subducting slab is not reliably determined and it may affect the final images. Thus in this study, we did not introduce the high-V subducting Pacific slab into the model. As shown in the next section, just because the high-V slab was not introduced into the initial model, we could acquire a variety of

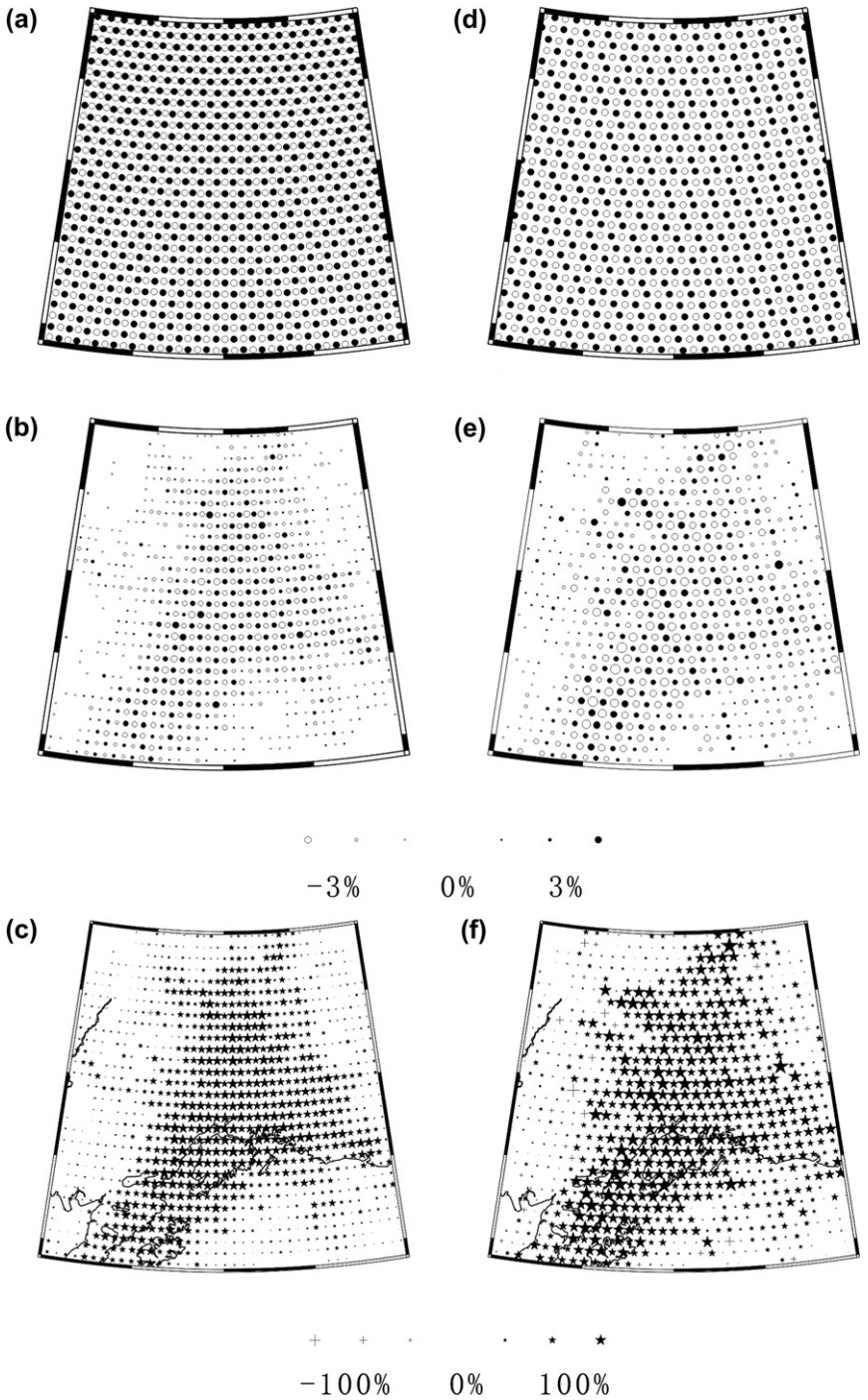

Fig. 6. The top diagrams are the input and output images in the checkerboard resolution test for the models with (a and b) regular grid parameterization and (d and e) irregular grid parameterization adopted, respectively. Another expression with relative variation measurement is shown at the bottom (c and f) (see the text). Stars and crosses indicate positive and negative values, meaning right and wrong recovery, respectively. The scale for the ratios is shown at the bottom.

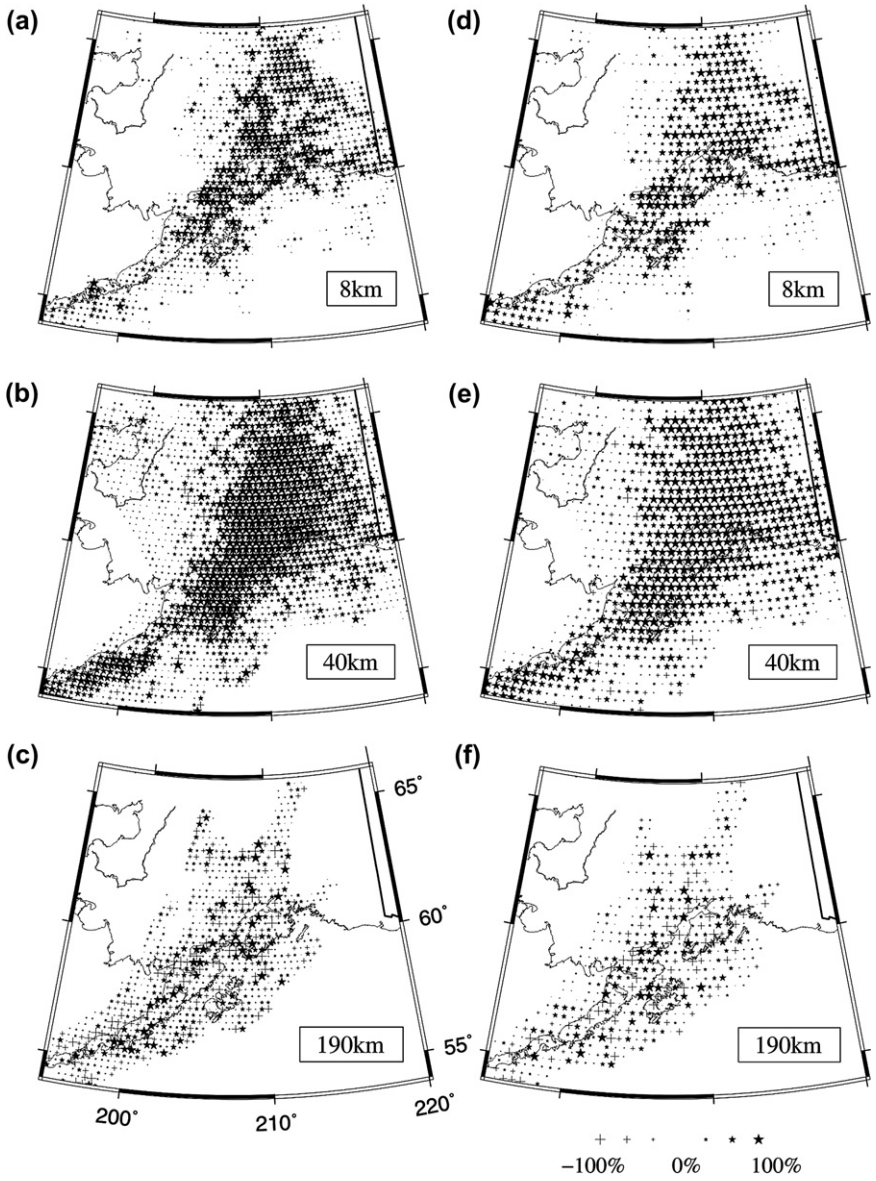

Fig. 7. Results of the checkerboard resolution test for the models with grid spacing of 0.25° (left) and that of 0.33° (right), respectively. Depth of each layer is exhibited in the lower right corner of each map. The scale for the ratios is shown at the bottom.

new findings, such as the existence of a thick low-V zone at the top of the slab instead of a simple high-V slab. It should be noted that it is not contradictory to introduce a priori information into the initial model before the inversion. Previous studies have testified that introducing a priori information can improve the final images (e.g., the tomographic studies of the Japan subduction zone by Zhao et al., 1992; Zhao and Hasegawa, 1993). For the tomographic study of Alaska, it will also be appropriate to introduce the subducting Pacific slab into the model if the slab geometry is clearly known.

4. Results and Discussion

Fig. 10 shows the P-wave velocity perturbations in horizontal planes. Earthquakes within a 1−10 km depth range from the slices are shown in each layer. The velocity perturbation was calculated from the average of the inverted velocity values in each layer. In the upper crust, we can see several low-V zones exist corresponding to the large Cenozoic sedimentary basins in southeastern Alaska, such as the Gulf of Alaska basin, Cook Inlet basin, and Minchumina Holitna-Tanana

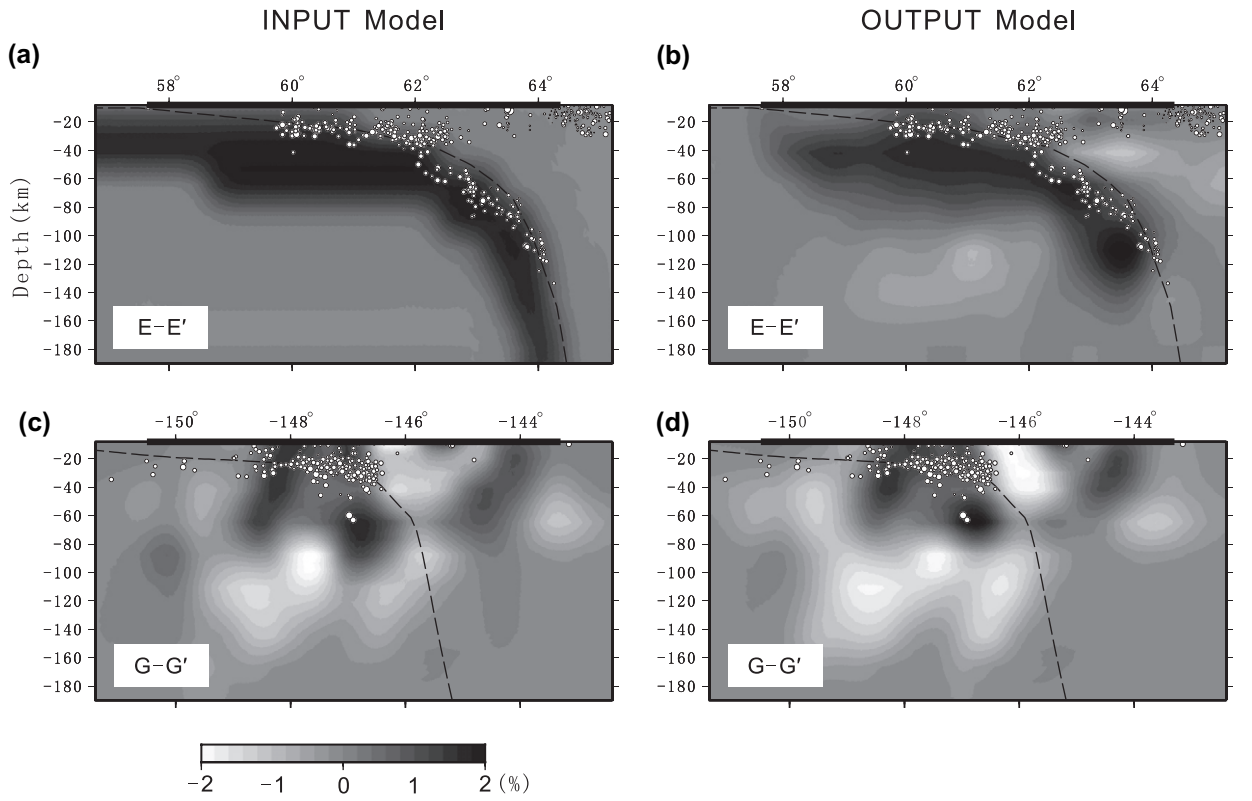

Fig. 8. Results of (a and b) the synthetic resolution test and (c and d) the restoring resolution test for profile E–E′ and G–G′. Locations of the profiles are shown in Fig. 9. Input and output models are shown on the left and right, respectively. White represents low-V while black denotes high-V. White circles indicate background earthquakes within a 20 km width from the cross-sections. Dashed lines exhibit the upper boundary of the subducting Pacific slab estimated by Zhao et al. (1995) for reference. The velocity perturbation scale is shown at the bottom.

Lowlands basin, from south to north. Between these basins are ultramafic bodies that are imaged as high-V anomalies. The most prominent high-V anomaly is located in the Chugach Mountains. In general, strong low-V anomalies appear in the crust and upper mantle wedge beneath the active volcanoes denoted by red triangles on the 8 km depth layer.

In the lower crust and upper mantle, the high-V anomalies outline the subducting Pacific slab well (Fig. 10). Most of the intermediate-depth earthquakes occur within the slab toward the continental side. The velocity within the slab is inhomogeneous, which may be due to the uneven ray path sampling besides the effect of heterogeneous thermal distribution (McKenzie, 1969; Hsui and Toksöz, 1979) or petrological variations structure (Ringwood, 1982).

The Denali fault appears to be a major crustal feature, and is particularly characterized by a prominent velocity contrast at 40 km depth (Fig. 10). In the 3-D velocity model made by Eberhart-Phillips et al. (2006), there is a low-V zone in the slab mantle at 110 km depth south of Cook Inlet, where the slab bends to become more parallel to the trench. In fact, our results show a prominent low-V zone in the slab mantle, which is considered to result from some pre-existing structural feature of the incoming Pacific plate or some mantle deformation process related to the bending (Eberhart-Phillips et al., 2006).

Several vertical cross-sections normal to the trench axis were made in order to map the geometry of the subducting Pacific slab, and the resolution of these images is also examined. Based on the cross-sections shown in Fig. 11, the features of our results are discussed for the subducting Pacific slab, arc magmatism and a specific terrane.

4.1. The subducting Pacific slab

Resolving the geometry of the subducting slab is very important for understanding the basic mechanics of subduction. As mentioned above, the first-order feature of the subducting Pacific slab shown in our results

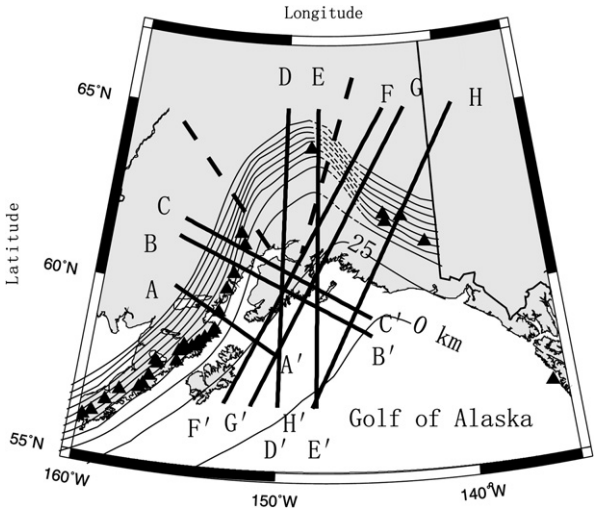

Fig. 9. Depth distribution of the upper boundary of the subducting Pacific plate in Alaska is shown as contour lines for reference in this study (in 25 km intervals, after Zhao et al., 1995). Thin dashed lines exhibit the upper boundary of the subducting Pacific slab estimated by Zhao et al. (1995). Eight heavy lines show the locations of the vertical cross-sections in Fig. 11. The Alaska subduction zone can be divided into three different parts, i.e., the western, middle and eastern parts. Their boundaries are roughly shown by thick dashed lines. Triangles are active volcanoes.

is that it is imaged as a high-V anomaly. However, the morphology of the subducting Pacific slab varies considerably in different cross-sections (Fig. 11). From the viewpoint of the slab seismicity, several researchers have suggested segmentation of the subducting Pacific plate (e.g., Ratchkovski and Hansen, 2002). From both the slab seismicity and our tomographic results, we suggest that the Alaska subduction zone can be divided into three parts, i.e., the western, middle and eastern parts, with boundaries between them near the Cook Inlet and the Kenai Peninsula (Fig. 9).

In the western part, the cross-sections across the Alaska−Aleutian subduction zone show typical images similar to other subduction zones (Fig. 11a−c). The subducting Pacific slab associated with a high-V anomaly can be seen clearly. The intermediate-depth earthquakes occur along or below the upper boundary of the slab, outlining the geometry of it. For the slab, however, the upper and lower boundaries of the high-V zone show an irregular shape in response to the imperfect ray coverage and parameterization. In this subduction zone the high-V slab is imaged as a roughly 50−80 km thick zone extending to 190 km in depth, the bottom of the velocity model. For the profile along line B−B′ (Fig. 11b), a strong velocity contrast allows us to evaluate the thickness of the descending slab more clearly, to be roughly 40 km at depths of 60−190 km.

However, heading eastward to view the cross-sections across the eastern end of the Alaska−Aleutian subduction zone, a very different character in the subducting slab is seen. In cross-sections D−D′ and E−E′, the high-V anomalies are visible, but a distinct low-V zone with most of the earthquakes overlies the high-V anomalies (Fig. 11). The synthetic resolution test confirmed that a slab-like high-V anomaly can be recovered well if there is a high-V anomaly in the input model (see Fig. 8a and b). From the horizontal velocity images at depths of 40−115 km (Fig. 10), we find this low-V zone is mainly located in the north of the Kenai Peninsula. In the profile D−D′ across the region north of Cook Inlet, the high-V anomaly relating to the subducting Pacific slab extends to the bottom of the model and departs from the earthquakes in the WBZ. On the other hand, the high-V anomaly shortens eastwards as the low-V zone thickens (see profile E−E′). A receiver function study shows that a 11−22 km thick low-V zone exists at the top of the slab (Ferris et al., 2003). Another suggestion comes from Eberhart-Phillips et al. (2006) who found a distinct low-V zone overlies the high-V zone to 140 km depth in the northern subduction zone, consistent with our results. This observation is very different from the slab images in other subduction zones, leading to the question: What is the low-V zone? We will discuss this issue in the next section.

For the eastern part, viewing sections F−F′, G−G′, and H−H′ beneath the transition zone and the Wrangell subduction zone, the high-V slab does not appear to extend deeper than 90 km depth and the seismicity is located solely within the high-V anomaly and ends abruptly at the strong gradient in P-wave velocity (Fig. 11). This region with no deep subducted slab was called the slab-free region by Eberhart-Phillips et al. (2006) who found that the high-V slab does not extend deeper than 60 km depth in the region east of Cordova in their results, denoting that there is a possibility that the slab extends deeper to the east by dipping more steeply. From our results, the Pacific slab subducts only down to 60−90 km depth, which contrasts with previous results that there is a seismically defined subducting Pacific slab to great depths (e.g., the Wrangell WBZ, Stephens et al., 1984). It is possible that few rays sample that region and so the deeper subducting slab cannot be imaged even if it exists.

Several previous studies have investigated the geometry of the subducting Pacific plate in Alaska (e.g., Yamaoka et al., 1986; Creager and Chiao, 1992). The proposed candidate models can be summarized as follows: the plate is continuous; the plate is torn and the western end of the Wrangell subducting plate is thrust

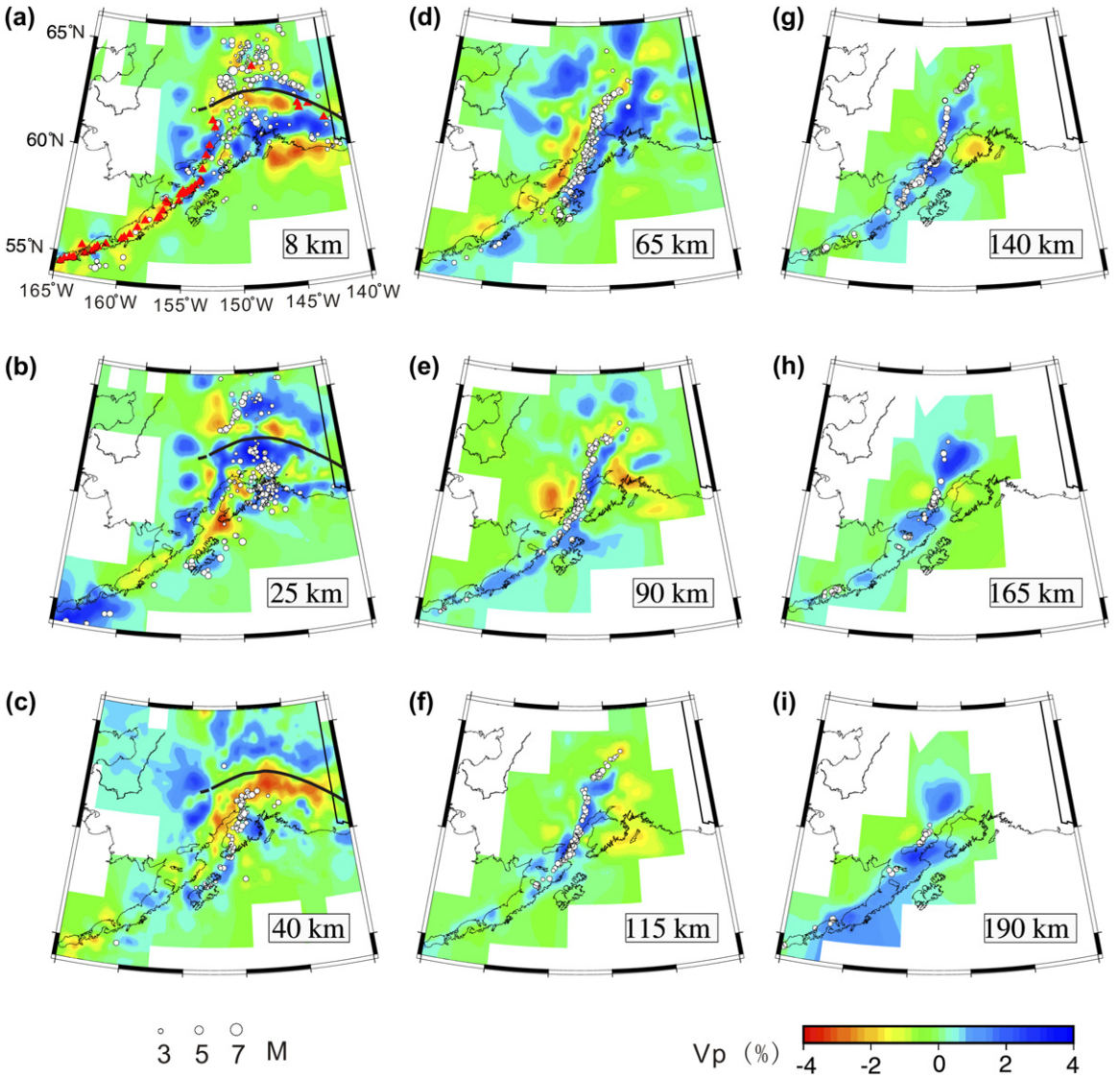

Fig. 10. P-wave velocity perturbations (in percent) in horizontal planes. Red and blue colors denote low and high velocities, respectively. Red triangles denote active volcanoes. Earthquakes within a 1–10 km depth range from the slices are superimposed in each layer. The depth of each layer is shown at the lower right in each map. Black lines at depths of 8, 25 and 40 km indicate the Denali Fault. The perturbation scale is shown at the bottom.

underneath the eastern end of the Alaska–Aleutian subducting plate; the plate is torn and pulled apart forming a gap between the Alaska–Aleutian and Wrangell subduction zones. In our results the Pacific plate appears to be continuous but becomes shallower eastward quickly. In addition, it is interesting to note that in the area northeast of the Wrangell subducting plate, there is a prominent high-V anomaly, and the question arises whether it is related to the Pacific plate.

As for the reason why the Pacific slab to the east cannot subduct so deeply, the mechanism behind this geometry has to be sought from morphology and knowledge of historic events such as slab window subduction in respect of the subduction of the Kula-Farallon related triple junction (Haeussler et al., 2003) or the motion direction change of the Pacific plate that occurred at ~43 Ma (Gordon and Jurdy, 1986). Further promising information on the evolution of the Pacific plate should come from teleseismic tomography, which can provide constraints on the deeper structure and the fate of the subducting Pacific slab under Alaska.

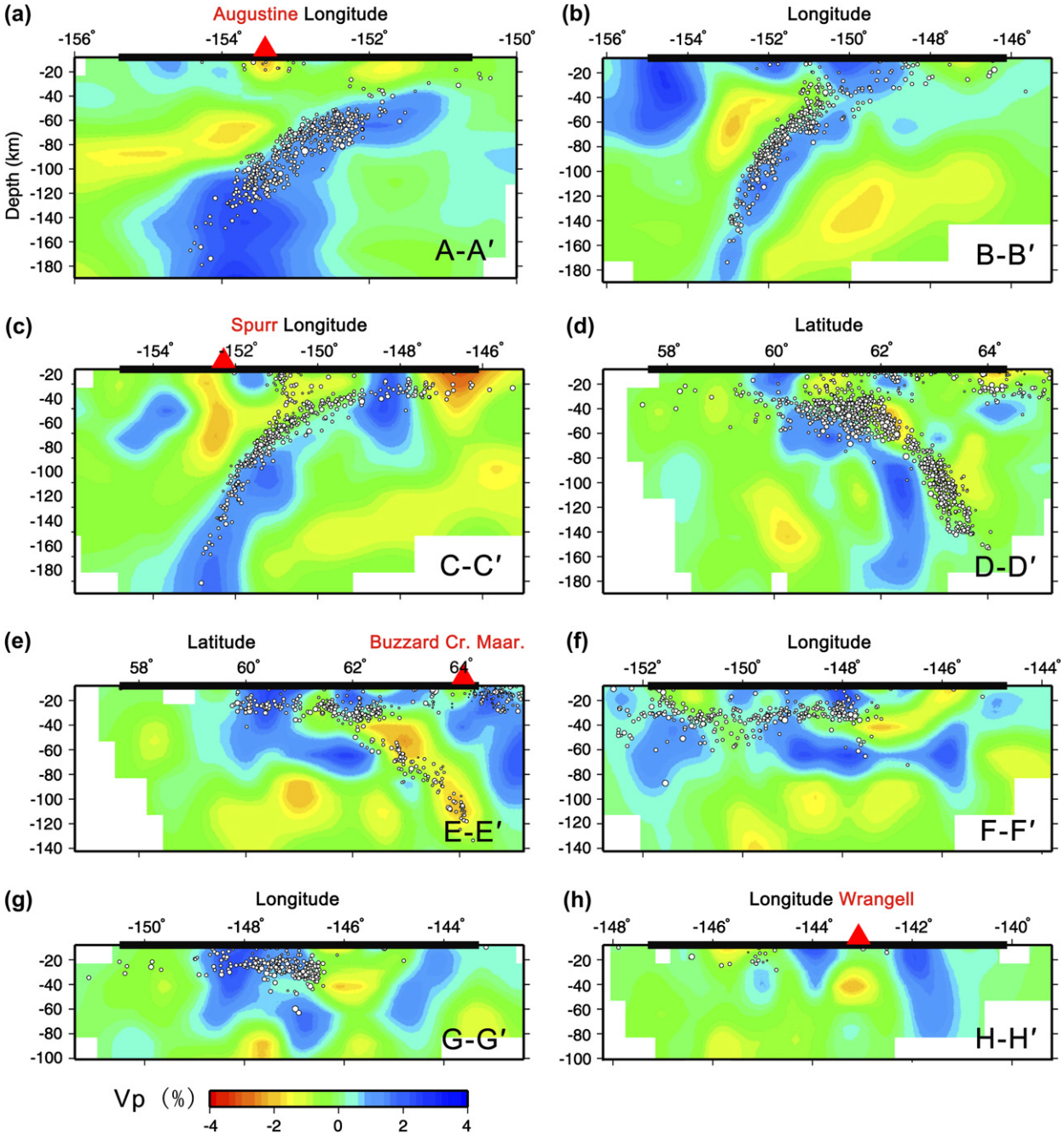

Fig. 11. Vertical cross-sections of P-wave velocity images (in percent) along eight lines shown in Fig. 9. Red color represents low-V while blue color denotes high-V. The regions with data absent were cut out. White circles indicate background earthquakes within a 20 km width from the cross-sections. Red triangles on the top of each section represent active volcanoes. The velocity perturbation scale is shown at the bottom. Note the various vertical exaggeration.

4.2. Arc volcanism

The subduction zone is one of the main regions of magmatism and volcanism in the earth. The three different forms of the subducting Pacific slab mentioned above result in three different forms of volcanism accordingly.

The volcanoes in the cross-sections through the western portion of the subducting Pacific slab in Fig. 11 are Aleutian volcanoes, exhibiting a general seismological

characteristic of subduction zones. The chain of strato volcanoes correlates strongly with the 100 km depth contour of the western WBZ (Gill, 1981). The low-V zones exist just beneath the active volcanoes and extend along inclined paths to a depth of about 100 km at the top of the descending slab, feeding the volcanoes above (see profiles A–A′ and C–C′). The contorted low-V zone is very likely to be the pathway for the magma or fluids that rise from the subducting slab to the volcanoes. The path for transportation is deflected in the direction of the plate boundary by a convective circulation process in the mantle wedge above the slab, similar to those in other subduction zones (e.g., Nakajima et al., 2001). The low velocity may be attributed to the dehydration of the downgoing slab at this depth range and to the serpentinization of the forearc upper mantle wedge, which might reduce the melting point of the rock above and trigger partial melting to produce arc magmas.

Along the western WBZ, however, volcanic activity ends abruptly with Spurr and Hayes, roughly 320 km west of the eastern termination of seismicity. This paucity of volcanism has been called the Denali volcanic gap (Nye, 1999). However, many studies have shown that the lack of volcanism does not arise from a lack of magmatism, and it is interesting to note our results for the cross-section E–E′ across the Buzzard Creek Maars at the eastern extreme of the volcanic gap (Fig. 11), which are a 3000 year old small-volume monogenetic volcanism erupting arc-basalt magmas. In this figure we can see that an anomaly with velocity lower than its surroundings shapes a conduit linking the Maars volcano to the thick LVZ. In addition, beneath the Denali volcanic gap, observations of high values of Poisson's ratio suggest that the mantle wedge contains melted material that is unable to reach the surface due to increased compression in the crust at the northern apex of the curved Denali fault (McNamara and Pasyanos, 2002). It is believed that the ongoing accretion of the Yakutat terrane to the southern Alaska margin is responsible for the compressed crust. In our results it is interesting that in the horizontal velocity image at the depth of 25 km (Fig. 10) there is a widely distributed high-V anomaly, which may represent the compressed crust inhibiting the rise of magma from supplying the surface volcanoes, or prescribe the "viscous nose" of the mantle wedge characterized mainly by high-Q and low temperatures (Stachnik et al., 2004; Abers et al., 2006) in this region. Alternatively, teleseismic observations on the BEAAR (Broadband Experiment across the Alaska Range) array to the west revealed the anisotropic fast directions are roughly parallel to the strike of the subducting plate north of the 70–75 km contour of the subducting plate, assuming a sub-lateral mantle flow in the mantle wedge due to a significant portion of the signal coming from the mantle wedge indicated by observations from local slab events (Christensen et al., 2003). Hence, the inferred sub-lateral mantle flow possibly finally finds its way out to the Maars volcano at the eastern end of the volcanic gap.

East of the Denali volcanic gap is the famous Wrangell volcanic field (WVF), which features an extensive volcanic terrain with a mass of lava flows that have been erupting during the past 26 Ma (Richter et al., 1990). In the WVF, Mt. Wrangell, a massive shield volcano, still occasionally signals its active presence with steam rising from its vents, and is still considered active. In the cross-section H–H′ across Mt. Wrangell (Fig. 11), a low-V anomaly exists below the volcano, but some distance from the ground surface, which may reflect the presence of a magma reservoir of partial melt beneath it. A similar low-V anomaly in the lower crust in the region is also supported by Eberhart-Phillips et al. (2006). Thus it is most likely that the current Wrangell volcanism is linked to magma at great depths. Unlike the Aleutian volcanoes in western Alaska, the Wrangell volcanism has been related to Miocene and younger Yakutat subduction (Plafker, 1987; Plafker and Berg, 1994). The steady dehydration of the subducting Yakutat slab may release fluids, which may migrate laterally from the seismogenic slab toward the WVF (Eberhart-Phillips et al., 2006).

4.3. Yakutat terrane

As mentioned above, our results reveal a distinct thick LVZ with a great number of earthquakes occurring within, overlying a high-V anomaly associated with the subducting Pacific slab in the north of the Kenai Peninsula. This kind of abnormal thick LVZ has attracted much attention. In an early seismic tomographic study of the Alaska region, Kissling and Lahr (1991) found that a large number of WBZ earthquakes occur in a zone of relatively low P-wave velocity, and the low-V anomaly is parallel to and overlies a region of relatively high P-wave velocity associated with descending lithosphere. This is very different from the finding of a sharp velocity contrast at the upper plate boundary for the subduction of the Pacific plate under Japan. They interpreted this thick low-V zone as a subducted oceanic crust.

A *b*-value analysis in this area indicates that a region of anomalously high *b*-value exists at depths of 90–100 km as a response to the dehydration using the slab (Wiemer and Benoit, 1996). In the receiver function study of the BEAAR data, Ferris et al. (2003) found large P-to-S conversion at the top of the slab is generated by

a 11−22 km thick low-V zone, as much as 20% slower than the surrounding mantle, and all intermediate-depth earthquakes that may be triggered by dehydration occur within the zone. Many studies in other subduction zones reveal that a 2−10 km thick zone with velocities 5−15% slower than the surroundings can be attributed to the subducting oceanic crust (Helffrich, 1996; Abers, 2000; Yuan et al., 2000; Cassidy and Ellis, 1993; Matsuzawa et al., 1986). Hence, the layer is too thick to represent metamorphosed oceanic crust because the LVZ thickness is at least twice that normally observed for oceanic crust (White et al., 1992; Mutter and Mytter, 1993). Accordingly, it may represent a thick serpentinized zone or, more likely, a thick exotic terrane subducting along with the Pacific plate (Ferris et al., 2003).

Later, a similar LVZ was observed from scattered wave migration by Rondenay et al. (2004), who proposed that the thickness of the LVZ varies from 20 km at shallow depths, where it is interpreted as oceanic crust plus an overlying serpentinized zone or coupled exotic terrane, to 8−10 km at 140 km depth, where it is interpreted as only oceanic crust. The thick LVZ was also highlighted in the recent counterpart seismic tomographic study by Eberhart-Phillips et al. (2006). In their results the thick LVZ was interpreted as the Yakutat terrane.

Southern Alaska is undergoing a series of exotic terranes. The Yakutat terrane, as the last terrane to arrive transported by the Pacific plate, docked about 26 Ma and impinges against the continent and resists subduction (Plafker, 1987). The terrane directly causes the formation of the composite plate, which consists of Eocene age oceanic crust of the Yakutat terrane coupled to the underlying Oligocene to late Eocene age Pacific plate (Fuis and Plafker, 1991; Brocher et al., 1994).

In our interpretation, all of the previous results lead us to believe that the extensive and thick LVZ is most likely the oceanic crust plus an overlying serpentinized zone and the coupled Yakutat terrane. If this is true, the buoyancy of the thickened crust causes crustal compression that leads to slab flattening, mountain building in the Alaska Range and perhaps the shutting off of magmatism. This may interpret the Yakataga seismic gap (Page et al., 1989), the Denali volcanic gap (Nye, 1999), and the generation of giant earthquakes such as the M 9.2 Alaska earthquake in 1964.

5. Conclusions

A detailed three-dimensional P-wave velocity structure to a depth of approximately 200 km in Alaska was obtained. By the use of an irregular grid parameterization in the model, the number of grid nodes increases from north to south in the study area so that the spacing between grid nodes is approximately the same in the longitude direction. Checkerboard resolution tests suggest irregular grids can provide a uniform resolution for better judgment of the final images, since denser grids may decrease the final resolution to the north. In addition, we did not introduce the slab into the initial model because the geometry of the subducting Pacific slab is still unclear.

Our results suggest that the tomographic image of the upper crust correlates well with the major surface geological features. The subducted Pacific plate is imaged as a high-V anomaly to the bottom of the model in most regions and a widespread low-V zone exists in the mantle beneath the high-V slab. However, a series of vertical cross-sections reveal that the geometry of the subducting Pacific slab is very complicated. Based on its geometry, we suggest the subducting Pacific plate in Alaska can be divided into three different parts.

In the western part in the Alaska−Aleutian subduction zone, the subducting Pacific plate is clearly visible as a 50−80 km thick continuous high-V zone. Inclined low-V anomalies extend from the top of the slab to the surface beneath volcanoes, which may reflect the arc magma caused by the slab dehydration and convective circulation process in the mantle wedge, similar to those in other subduction zones. In the central part we found that a thick LVZ is imaged at the top of the subducting Pacific slab beneath north of the Kenai peninsula with a great number of earthquakes occurring within, which are believed to most likely be the oceanic crust plus an overlying serpentinized zone and the coupled Yakutat terrane subducted along with the Pacific slab. The existence of the exotic terrane makes the underlying Pacific plate more complicated, and the thickened crust drives crustal compression that directly inhibits the rise of magma through it to supply the surface volcanoes as far as the Buzzard Creek Maars, leading to the formation of the Denali volcanic gap. However, in the eastern part where the plate boundary type between the Pacific and North American plates changes from oblique subduction to strike-slip, the subducted Pacific plate is only imaged as a high-V slab down to 60−90 km, which is different from a previous study that suggests a seismically defined subducting Pacific slab to great depths. In addition, the volcanism in this region is still considered to be related to the subducted Yakutat terrane than simple arc volcanism.

Acknowledgments

This work was partially supported by a research grant (Kiban-A 17204037) from the Japanese Ministry

of Education and Science to D. Zhao. The data used in this study were supplied by the AEIC seismic network in Alaska jointly run by the Geophysical Institute of UAF and the US Geological Survey. We thank Prof. K. Shibuya and two anonymous reviewers for their thoughtful review comments, which improved the manuscript. We appreciate Dr. Baoshan Wang for the thoughtful discussion.

References

Abers, G.A., 2000. Hydrated subducted crust at 100−250 km depth. Earth Planet. Sci. Lett. 176, 323−330.

Abers, G.A., van Keken, P.E., Kneller, E.A., Ferris, A., Stachnik, J.C., 2006. The thermal structure of subduction zones constrained by seismic imaging: implications for slab dehydration and wedge flow. Earth Planet. Sci. Lett. 241, 387−397.

Brocher, T.M., Fuis, G.S., Fisher, M.A., Plafker, G., Moses, M.J., Taber, J.J., Christensen, N.I., 1994. Mapping the megathrust beneath the northern Gulf of Alaska using wide-angle seismic data. J. Geophys. Res. 99, 11663−11685.

Cassidy, J.F., Ellis, R.M., 1993. S wave velocity structure of the northern Cascadia subduction zone. J. Geophys. Res. 98, 4407−4421.

Christensen, D.H., Abers, G.A., McKnight, T.L., 2003. Mantle anisotropy beneath the Alaska Range inferred from S-wave splitting observations: results from BEAAR. EOS Trans. AGU 84. S31C-0782.

Creager, K.C., Chiao, L.Y., 1992. Membrane deformation rate and geometry of Aleutian-Alaska subduction. In: Wadati Conference on Great Subduction Earthquakes, 16−19 September 1992, Geophysical Institute, University of Alaska Fairbanks, Fairbanks, Alaska, 27 p.

Dziewonski, A.M., Gilbert, F., 1976. The effect of small, aspherical perturbations on travel times and a re-examination of the corrections for ellipticity. Geophys. J. R. Astr. Soc. 44, 7−17.

Eberhart-Phillips, D., Christensen, D.H., Brocher, T.M., Hansen, R., Ruppert, N.A., Haeussler, P.J., Abers, G.A., 2006. Imaging the transition from Aleutian subduction to Yakutat collision in central Alaska, with local earthquakes and active source data. J. Geophys. Res. 111, B11303, doi:10.1029/2005JB004240.

Ferris, A., Abers, G.A., Christensen, D.H., Veenstra, E., 2003. High resolution image of the subducted Pacific (?) plate beneath central Alaska, 50−150 km depth. Earth Planet. Sci. Lett. 214, 575−588.

Fuis, G.S., Plafker, G., 1991. Evolution of deep structure along the Trans-Alaska Crustal Transect, Chugach Mountains and Copper River Basin, southern Alaska. J. Geophys. Res. 96, 4229−4253.

Gill, J., 1981. Orogenic Andesites and Plate Tectonics. Springer Verlag, New York, 390 p.

Gordon, R.G., Jurdy, D.M., 1986. Cenozoic global plate motions. J. Geophys. Res. 91, 12389−12406.

Haeussler, P.J., Bradley, D.C., Wells, R.E., Miller, M.L., 2003. Life and death of the Resurrection plate: evidence for its existence and subduction in the northeastern Pacific in Paleocene−Eocene time. Geol. Soc. Am. Bull. 15, 867−880.

Helffrich, G.R., 1996. Subducted lithospheric slab velocity structure; observations and mineralogical inferences. In: Bebout, G.E., Scholl, D.W., Kirby, S.H., et al. (Eds.), Subduction Top to Bottom. American Geophysical Union, pp. 215−222.

Hsui, A.T., Toksöz, M.N., 1979. The evolution of thermal structures beneath a subduction zone. Tectonophysics 60, 43−60.

Humphreys, E., Clayton, R.W., 1988. Adaptation of back projection tomography to seismic travel time problems. J. Geophys. Res. 93, 1073−1085.

Jones, D.L., Silberling, N.J., Coney P.J., Plafker, G., (1987). Lithotectonic terrane map of Alaska (west of the 41st meridian), US Geol. Surv. Misc. Field stud. Map, MF-1874-A.

Kennett, B.L.N., Engdahl, E.R., 1991. Travel times for global earthquake location and phase identification. Geophys. J. Int. 105, 429−465.

Kissling, E., Lahr, J.C., 1991. Tomographic image of the Pacific slab under southern Alaska. Eclogae Geol. Helv. 84, 297−315.

Lahr, J.C., Plafker, G., 1980. Holocene Pacific-North American plate interaction in southern Alaska: implications for the Yakataga seismic gap. Geology 8, 483−486.

Matsuzawa, T., Umino, N., Hasegawa, A., Takagi, A., 1986. Upper mantle velocity structure estimated from PS-converted waves beneath the northeastern Japan arc. Geophys. J. R. Astron. Soc. 86, 767−787.

McKenzie, D.P., 1969. Speculations on the consequences and causes of plate motions. Geophys. J. R. Astron. Soc. 18, 1−32.

McNamara, D.E., Pasyanos, M.E., 2002. Seismological evidence for a sub-volcanic arc mantle wedge beneath the Denali volcanic gap, Alaska. Geophys. Res. Lett. 29, doi:10.1029/2001GL014088.

Mutter, C.Z., Mytter, J.C., 1993. Variations in thickness of layer 3 dominate oceanic crustal structure. Earth Planet. Sci. Lett. 117, 295−317.

Nakajima, J., Matsuzawa, T., Hasegawa, A., Zhao, D., 2001. Three-dimensional structure of Vp, Vs and Vp/Vs beneath northeastern Japan: implications for arc magmatism and fluids. J. Geophys. Res. 106, 21843−21858.

Nye, C., 1999. The Denali Volcanic Gap − magmatism at the eastern end of the Aleutian Arc. Eos 80 (46 suppl.), 1203.

Page, R.A., Stephens, C.D., Lahr, J.C., 1989. Seismicity of the Wrangell and Aleutian Wadati-Benioff zones and the North American plate along the Trans-Alaska crustal Transect, Chugach Mountains and Copper river basin, Southern Alaska. J. Geophys. Res. 94, 16059−16082.

Paige, C., Saunders, M., 1982. LSQR: an algorithm for sparse linear equations and sparse least squares. Assoc. Comput. Mach. Trans. Math. Software 8, 43−71.

Plafker, G., 1987. Regional geology and petroleum potential of the northern Gulf of Alaska continental margin. In: Scholl, D.W., Grantz, A., Vedder, J.G. (Eds.), Geology and Resource Potential of the Continental Margin of Western North America and Adjacent Ocean Basins − Beaufort Sea to Baja California. Earth Sciences Series, vol. 6. Circum-Pacific Council for Energy and Mineral Resources, Houston, Texas, pp. 229−268.

Plafker, G., Berg, H.C., 1994. Overview of the geology and tectonic evolution of Alaska. In: Plafker, G., Berg, H.C. (Eds.), The Geology of North America. The Geology of Alaska, vol. G-1. Geological Society of America, Boulder, CO, pp. 989−1021.

Ratchkovski, N.A., Hansen, R.A., 2002. New evidence for segmentation of the Alaska subduction zone. Bull. Seism. Soc. Am. 92, 1754−1765.

Richter, D.H., Smith, J.G., Lanphere, M.A., Dalrymple, G.B., Reed, B.L., Shew, N., 1990. Age and progression of volcanism, Wrangell volcanic field, Alaska. Bull. Volcanol. 53, 29−44.

Ringwood, A.E., 1982. Phase transformations and differentiation in subducted lithosphere: implications for mantle dynamics, basalt petrogenesis, and crustal evolution. J. Geol. 90, 611−643.

Rondenay, S., Abers, G.A., Ferris, A., 2004. A new, high-resolution seismic profile of the central-Alaskan subduction zone. Eos Trans. AGU 85 (17). Jt. Assem. Suppl., Abstract U54A-05.

Stachnik, J.C., Abers, G.A., Christensen, D.H., 2004. Seismic attenuation and mantle wedge temperatures in the Alaska subduction zone. J. Geophys. Res. 109, B10304, doi:10.1029/2004JB003018.

Stephens, C.D., Fogleman, K.A., Lahr, J.C., Page, R.A., 1984. Wrangell Benioff zone, southern Alaska. Geology 12, 373–376.

White, R.S., McKenzie, D., O'Nions, R.K., 1992. Oceanic crustal thickness from seismic measurements and rare earth element inversions. J. Geophys. Res. 97, 19683–19715.

Wiemer, S., Benoit, J.P., 1996. Mapping the b-value anomaly at 100 km depth in the Alaska and New Zealand subduction zones. Geophys. Res. Lett. 23, 1557–1560.

Yamaoka, K., Fukao, Y., Kumazawa, M., 1986. Spherical shell tectonics: effects of sphericity and inextensibility on the geometry of the descending lithosphere. Rev. Geophys. 24, 27–53.

Yuan, X., Sobolev, S.V., Kind, R., et al., 2000. Subduction and collision processes in the Central Andes constrained by converted seismic phases. Nature 408, 958–961.

Zhao, D., Hasegawa, A., Horiuchi, S., 1992. Tomographic imaging of P and S wave velocity structure beneath northeastern Japan. J. Geophys. Res. 97, 19909–19928.

Zhao, D., Hasegawa, A., 1993. P wave tomographic imaging of the crust and upper mantle beneath the Japan Islands. J. Geophys. Res. 98, 4333–4353.

Zhao, D., Hasegawa, A., Kanamori, H., 1994. Deep structure of Japan subduction zone as derived from local, regional and teleseismic events. J. Geophys. Res. 99, 22313–22329.

Zhao, D., Christensen, D., Pulpan, H., 1995. Tomographic imaging of the Alaska subduction zone. J. Geophys. Res. 100, 6487–6504.

Zhao, D., Xu, Y., Wiens, D., et al., 1997. Depth extent of the Lau back-arc spreading center and its relation to subduction processes. Science 278, 254–257.